

Switchable and selective detection of Zn²⁺ or Cd²⁺ in living cells based on 3'-O-substituted arrangement of benzoxazole-derived fluorescent probes†

 Cite this: *Chem. Commun.*, 2014, 50, 7514

 Received 29th March 2014,
 Accepted 19th May 2014

DOI: 10.1039/c4cc02335h

www.rsc.org/chemcomm

 Yongqian Xu,^{*a} Liangliang Xiao,^a Shiguo Sun,^{*a} Zhichao Pei,^a Yuxin Pei^a and Yi Pang^b

Two benzoxazole-derived ESIPT fluorescent sensors E1 and E2 show highly selective detection of Zn²⁺ and Cd²⁺, respectively, in aqueous solution and living cells. The selectivity switching from Zn²⁺ to Cd²⁺ is attributed to the different binding mode which is dependent on the 3'-O-substituted arrangement.

The zinc ion (Zn²⁺), as the second most abundant transition metal ion in the human body, plays a very important role in biological processes such as gene transcription, immune function, pathology, neural signal transmission, as well as catalysis of proteins.¹ Zinc imbalance is associated with a number of pathological disorders including Alzheimer's disease, epilepsy, Parkinson's disease, ischemic stroke and infantile diarrhea.² On the other hand, the cadmium ion (Cd²⁺), being in the same group as the zinc ion in the periodic table, is a heavy metal and widely used in industry and agriculture including the production of electroplating, metallurgy, batteries, etc.³ Cd²⁺ is highly toxic and can be easily absorbed and accumulated by plants and other organisms, leading to renal dysfunction, calcium metabolism disorders and cancers.^{3c} Thereby the measurement of Zn²⁺ or Cd²⁺ in physiological media has been considered as an essential factor and the addressed target in these relative diseases. Among the methods developed for Zn²⁺ or Cd²⁺ sensing, fluorescent probes have attracted considerable attention due to their simple operation, high sensitivity, noninvasiveness and real time detection.⁴ Hitherto, significant effort has been devoted to the development of fluorescent sensors for Zn²⁺ or Cd²⁺ with successful applications to image in living cells.⁵ However, most of them suffered from limited selectivity over biologically abundant metal ions like Fe²⁺/Fe³⁺ and Cu²⁺ due to the moderate coordination nature of Zn²⁺ and the use of di-2-picolyamine (DPA) as a chelator.⁶ In addition, Zn²⁺ and Cd²⁺ have similar properties that lead to a similar binding mode to acceptors of sensors, providing

identical spectral changes that make it difficult to discriminate them. Thus it is a large challenge to design the sensors for highly selective detection of Zn²⁺ or Cd²⁺. Although many fluorescent sensors with modified receptors can efficiently and highly detect Zn²⁺ or Cd²⁺, there is no reliable design guide for selective recognition of Zn²⁺ or Cd²⁺. Recently, Xu *et al.* reported a fluorescent sensor with a tautomerization-based transformable receptor.¹⁰ Although the sensor shows distinct fluorescence changes to discriminate between Zn²⁺ and Cd²⁺ because of different binding modes (Zn²⁺ in an imidic acid form, Cd²⁺ in an amide tautomeric form), it can only recognize Zn²⁺ in the presence of both Zn²⁺ and Cd²⁺ due to different binding affinity. In order to study and understand the binding properties and diversity of Zn²⁺ and Cd²⁺, it is necessary to use a structure-tuned receptor to ensure switchable selectivity for Zn²⁺ or Cd²⁺.

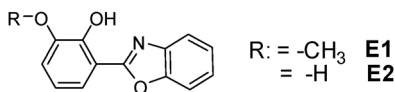
Recently, fluorescent sensors based on excited-state intramolecular proton transfer (ESIPT), as seen from 2-(2'-hydroxyphenyl)benzoxazole (HBO), have attracted more interest.⁷ ESIPT sensors exhibit dual emissions from both the excited enol and keto tautomers. Fluorescent sensing of metal ions could be realized by prohibiting ESIPT through the coordination of metal ions with ESIPT centers, resulting in detectable spectral changes.⁷ Compared with the widely used photo-induced electron transfer (PET) mechanism for Zn²⁺ or Cd²⁺, the fluorescent sensors based on ESIPT can afford many advantages including dual fluorescence intensity changes and large Stokes shift.⁹ They can detect metal ions with ratiometric fluorescent response and a near infrared (NIR) fluorescent signal (700–900 nm), providing the self-calibration function and avoiding photodamage, scattering light and strong interference derived from short wavelength emission in biological media.⁸

Herein, we present two ESIPT fluorescent sensors **E1** and **E2** for Zn²⁺ and Cd²⁺ sensing, respectively (Scheme 1). Both of them show high sensitivity and selectivity in aqueous solution. Compared with **E1**, **E2** has no methyl group at the 3'-hydroxyl position. With and without the methyl group, the selectivity of the sensor switches from Zn²⁺ to Cd²⁺. As a proof-of-principle method, substituent arrangement-induced selectivity switching has been proved, which would be helpful to design fluorescent sensors for efficient discrimination between Zn²⁺ and Cd²⁺.

^a College of Science, Northwest A&F University, Yangling, Shaanxi, P.R. China 712100. E-mail: xuyq@mwsuaf.edu.cn, sunsg@mwsuaf.edu.cn

^b Department of Chemistry & Maurice Morton Institute of Polymer Science, The University of Akron, Akron, OH, 44325, USA

† Electronic supplementary information (ESI) available: Details of the synthetic procedure and additional spectra. See DOI: 10.1039/c4cc02335h

Scheme 1 Structure of **E1** and **E2**.

The detailed synthetic procedure is described in the ESI†. Briefly, **E1** was readily synthesized by condensation reaction between *O*-vanillin and 2-aminophenol. Subsequently, **E2** could be obtained from the demethylation of **E1** in the presence of BBr_3 . All these compounds were fully characterized by ^1H NMR, ^{13}C NMR and HRMS.

In $\text{CH}_3\text{CN}/\text{HEPES}$ buffer (1:1, v/v, pH 7.4), **E1** exhibited one absorption peak at 325 nm, while upon addition of Zn^{2+} , the absorption at 325 nm gradually decreased, whereas a new absorption peak appeared at 370 nm with a well-defined isosbestic point at 340 nm (Fig. S1a, ESI†). Accordingly, upon excitation at 305 nm, the maximum emission at 380 nm stabilized and a new emission peak at 455 nm appeared, the intensity of which evidently increased upon successive addition of Zn^{2+} (Fig. S2, ESI†). The two emission bands at 380 and 455 nm can be attributed to the normal isomer (N^* emission) and tautomer (T^* emission) of **E1**, respectively.⁷ The observed fluorescence increase of the tautomer indicated that the Zn^{2+} binding is beneficial for the stability of the tautomer. The new emission peak can be used for the ratiometric fluorescent measurement of Zn^{2+} . Interestingly, upon excitation at 360 nm, except for an emission band at 455 nm, a new NIR emission band at 880 nm appeared (Fig. 1). Their fluorescence intensities gradually increased linearly with addition of Zn^{2+} (Fig. S3, ESI†). After addition of 1 equivalent of Zn^{2+} , the fluorescence quantum yield of **E1** changes from 0.0206 to 0.34. The Job's plot revealed 1:1 stoichiometry for the binding between **E1** and Zn^{2+} (Fig. S4, ESI†). The binding constant was calculated to be $6.51 \times 10^4 \text{ M}^{-1}$ with a detection limit of $1.63 \times 10^{-8} \text{ M}$. The selectivity of **E1** to various metal ions was further examined. As shown in Fig. S6 (ESI†), only Zn^{2+} promotes significant fluorescence intensity enhancement at 458 and 880 nm, whereas other metal ions cause no detectable spectral change except that Cu^{2+} induces somewhat fluorescence quenching. To explore the possible utility of **E1** as a fluorescent sensor for Zn^{2+} , competitive experiments were carried out in the presence of 20 equivalents of Zn^{2+} and 20 equivalents of various other cations (Fig. 2). Although Cd^{2+} exerts a weak increasing effect on the probe, the little interference can be eliminated by cysteine (Cys) that is abundant *in vivo*.¹⁰ The **E1** + Zn^{2+} complex is stable in the presence of Cys while the **E1** + Cd^{2+} complex is dissociated owing to the competition

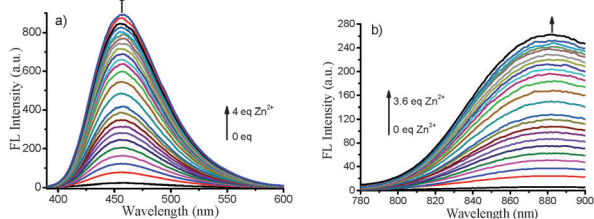


Fig. 1 The fluorescent spectral change of **E1** (10 μM) in short and long wavelength regions upon addition of Zn^{2+} in $\text{CH}_3\text{CN}/\text{HEPES}$ buffer (1:1, v/v, pH 7.4), $\lambda_{\text{ex}} = 360 \text{ nm}$.

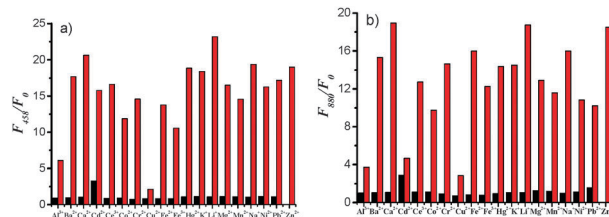


Fig. 2 Emission intensity of **E1** (10 μM) at 458 (a) and 880 nm (b) in $\text{CH}_3\text{CN}/\text{HEPES}$ buffer (1:1, v/v, pH 7.4) in the presence of different metal ions (200 μM) with the excitation at 360 nm (blank bar). Red bars represent the intensity with subsequent addition of Zn^{2+} ions (200 μM).

of Cys (Fig. S7, ESI†). These results suggested that **E1** shows excellent binding selectivity for Zn^{2+} and can detect Zn^{2+} with NIR emission.

Compared with **E1**, **E2** only lost the methyl group at the 3'-hydroxyphenyl position. Under identical conditions, **E2** shows similar UV-Vis spectral change upon addition of Cd^{2+} with a well-defined isosbestic point at 350 nm (Fig. S1b, ESI†). Upon excitation at 305 nm, **E2** has two maximum emission bands at 360 and 468 nm (Fig. S8, ESI†), assigned to the normal isomer (N^* emission) and tautomer (T^* emission), respectively. When excited at 360 nm, the fluorescence intensity at 468 nm evidently increased with successive addition of Cd^{2+} . The fluorescence quantum yield (Φ) increased from 0.0012 to 0.032 in the presence of 1 equivalent of Cd^{2+} . Its fluorescence intensity gradually increased linearly with addition of Cd^{2+} (Fig. 3a and Fig. S9, ESI†). The Job's plot revealed 1:1 stoichiometry for the binding between **E2** and Cd^{2+} (Fig. S10, ESI†). The binding constant was calculated to be $1.99 \times 10^4 \text{ M}^{-1}$ and the detection limit was $1.33 \times 10^{-7} \text{ M}$. In sharp contrast to **E1**, **E2** showed excellent selectivity to Cd^{2+} . Competitive experiments were carried out in the presence of 20 equivalents of Cd^{2+} and 20 equivalents of various other cations (Fig. 3b). Except that Mg^{2+} induced a little fluorescence increase, other various metal ions including Zn^{2+} ions caused no detectable spectral change at 469 nm. The result suggested that **E2** can highly detect Cd^{2+} without interference by Zn^{2+} . Moreover, competitive experiments were carried out in the presence of Cys, showing that there is no interference from Cys for probe **E2** to detect Cd^{2+} ions possibly due to the stronger binding capability between **E2** and Cd^{2+} (Fig. S21 and S22, ESI†). Both of them are pH independent in the range of 7–8, demonstrating that they can detect metal ions in biological environments (Fig. S11 and S12, ESI†).

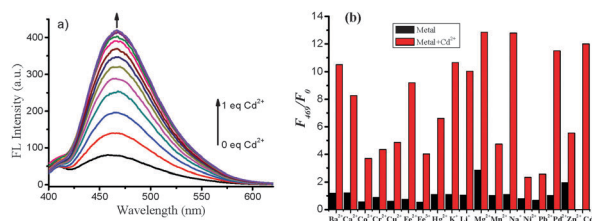


Fig. 3 (a) Fluorescence emission spectra of **E2** (10 μM) upon addition of Cd^{2+} in $\text{CH}_3\text{CN}/\text{HEPES}$ buffer (1:1, v/v, pH 7.4), $\lambda_{\text{ex}} = 360 \text{ nm}$; (b) emission intensity of **E2** (10 μM) at 469 nm in $\text{CH}_3\text{CN}/\text{HEPES}$ buffer (1:1, v/v, pH 7.4) in the presence of different metal ions (200 μM) with the excitation at 360 nm (blank bar). Red bars represent the intensity with subsequent addition of Cd^{2+} ions (200 μM).

Interestingly, the selectivity can be switched from Zn^{2+} to Cd^{2+} through a facial substituent effect of benzoxazole derivatives. To further evaluate the response nature and gain insight into the recognition mechanism for Zn^{2+} and Cd^{2+} , the ^1H NMR titration spectra of **E1** with Zn^{2+} and **E2** with Cd^{2+} were investigated. The chemical shift of the hydroxyl $-\text{OH}$ can be used to value whether the metal ion is bound to the hydroxyl oxygen. For **E1**, the $\text{Zn}-\text{O}$ bond results in the disappearance of the $-\text{OH}$ resonance peak at 11.20 with addition of 2 equivalents of Zn^{2+} in $\text{DMSO}-d_6$ (Fig. S13, ESI †). This result indicates that the $-\text{OH}$ group was involved in the binding with Zn^{2+} . In the case of **E2**, the Cd^{2+} binding results in the upfield shift of the $-\text{OH}$ proton at the 2' position from 11.10 to 11.07 and the downfield shift of the $-\text{OH}$ proton at the 3' position from 9.56 to 9.60 (Fig. S14, ESI †). The two different effects on the $-\text{OH}$ proton could be considered as a result of the Cd^{2+} binding. Through-bond propagation increases the electron density on the hydroxyl group at the 2' position and produces a shielding effect. While a through-space effect increases the polarization of the hydroxyl group at the 3' position, the partial positive charge causes a deshielding effect and downfield shift of its proton.¹¹ The non-vanishing of $-\text{OH}$ protons at 2' and 3' positions after addition of Cd^{2+} suggested that the two hydroxyl groups do not participate in the binding with Cd^{2+} . The strong intramolecular hydrogen bonding possibly prevents Cd^{2+} ions from binding with hydroxyl groups. The proposed binding modes of **E1** with Zn^{2+} and **E2** with Cd^{2+} were observed, from which different ion-induced binding profiles are attributed to different selectivity (Scheme S1, ESI †). More direct evidence was obtained from the ESI mass spectra, where the ion peak at m/z 510.31 (Fig. S15, ESI †) corresponded to the molecular ion peak of $[\text{E1}-\text{H} + \text{Zn}^{2+} + 2\text{CH}_3\text{OH} + \text{H}_2\text{O} + \text{ClO}_4^- + \text{Na}^+]$ (calcd = 510.15). For **E2**, the peak at m/z 451.74 (Fig. S16, ESI †) corresponded to the molecular ion peak of $[\text{E2} + \text{Cd}^{2+} + \text{CH}_3\text{OH} + \text{H}_2\text{O} + \text{NO}_3^-]$ (calcd = 451.69).

To further investigate the biological application of **E1** and **E2**, a fluorescence microscopy experiment in living cells was carried out. When ovarian cancer cells (SKOV-3) were incubated with 10 μM **E1** and **E2** in culture medium at 37 $^\circ\text{C}$ for 1 h, relatively, no detectable emission was observed. After incubation with Zn^{2+} and Cd^{2+} for **E1** and **E2**, respectively, strong green emission can be clearly seen, indicating a very good cellular uptake and

efficient fluorescent detection in living cells (Fig. 4 and Fig. S17, ESI †). Moreover, NIR red emission can be detected in the case of **E1** treated with Zn^{2+} .

In summary, two kinds of benzoxazole-derived ligands **E1** and **E2**, being different at a methyl substituent, have been presented. For **E1**, it can selectively detect Zn^{2+} in buffer solution and living cells with fluorescence intensity increasing at 455 and 880 nm. The selectivity can be further improved without interference from Cd^{2+} in the presence of biological Cys. For **E2**, it shows excellent selectivity toward Cd^{2+} and can be applied for living cell imaging. The possible binding modes between them were investigated by ^1H NMR titration spectra, from which the reasons and recognition mechanisms were interpreted. As a proof-of-principle method, substituent arrangement-induced selectivity switching would be helpful in the design of fluorescent sensors for other metal ions.

This work was supported by the National Natural Science Foundation of China (Grant No. 21206137), the Scientific Research Foundation of Northwest A&F University (Z111021103 and Z111021107) and the Fundamental Research Funds for the Central Universities (2452013py014).

Notes and references

- (a) C. J. Frederickson, J. Y. Koh and A. I. Bush, *Nat. Rev. Neurosci.*, 2005, **6**, 449; (b) J. M. Berg and Y. Shi, *Science*, 1996, **271**, 1081; (c) M. Lu and D. Fu, *Science*, 2007, **317**, 1746.
- (a) A. I. Bush, *Curr. Opin. Chem. Biol.*, 2000, **4**, 184; (b) C. F. Walk and R. E. Black, *Annu. Rev. Nutr.*, 2004, **24**, 255.
- (a) S. Satarug and M. R. Moore, *Environ. Health Perspect.*, 2004, **112**, 1099; (b) M. Waisberg, P. Joseph and B. Hale, *Toxicology*, 2003, **192**, 95; (c) R. A. Goyer, J. Liu and M. P. Waalkes, *Biomaterials*, 2004, **17**, 555.
- (a) Z. Xu, K.-H. Baek, H. N. Kim, J. Cui, X. Qian, D. R. Spring, I. Shin and J. Yoon, *J. Am. Chem. Soc.*, 2010, **132**, 601; (b) A. P. de Silva, H. Q. N. Gunaratne, T. Gunnlaugsson, A. J. M. Huxley, C. P. McCoy, J. T. Rademacher and T. E. Rice, *Chem. Rev.*, 1997, **97**, 1515; (c) W. Xuan, C. Chen, Y. Cao, W. He, W. Jiang, K. Liu and W. Wang, *Chem. Commun.*, 2012, **48**, 7292–7294; (d) M. Collot, C. Loukou, A. V. Yakovlev, C. D. Wilms, D. Li, A. Evrard, A. Zamaleeva, L. Bourdieu, J. F. Leger, N. Ropert, J. Eilers, M. Oheim, A. Feltz and J. M. Mallet, *J. Am. Chem. Soc.*, 2012, **134**, 14923–14931; (e) Z. Xu, X. Liu, J. Pan and D. R. Spring, *Chem. Commun.*, 2012, **48**, 4764.
- (a) C. Lu, Z. Xu, J. Cui, R. Zhang and X. Qian, *J. Org. Chem.*, 2007, **72**, 3554; (b) L. Xue, C. Liu and H. Jiang, *Org. Lett.*, 2009, **11**, 1655–1658.
- (a) X. Zhang, K. S. Lovejoy, A. Jasanoff and S. J. Lippard, *Proc. Natl. Acad. Sci. U. S. A.*, 2007, **104**, 10780; (b) B. A. Wong, S. Friedle and S. J. Lippard, *J. Am. Chem. Soc.*, 2009, **131**, 7142; (c) X. Zhang, D. Hayes, S. J. Smith, S. Friedle and S. J. Lippard, *J. Am. Chem. Soc.*, 2008, **130**, 15788; (d) E. Tomat, E. M. Nolan, J. Jaworski and S. J. Lippard, *J. Am. Chem. Soc.*, 2008, **130**, 15776; (e) J. E. Kwon, S. Lee, Y. You, K.-H. Baek, K. Ohkubo, J. Cho, S. Fukuzumi, I. Shin, S. Y. Park and W. Nam, *Inorg. Chem.*, 2012, **51**, 8760; (f) Y. You, S. Lee, T. Kim, K. Ohkubo, W.-S. Chae, S. Fukuzumi, G.-J. Jhon, W. Nam and S. J. Lippard, *J. Am. Chem. Soc.*, 2011, **133**, 18328; (g) Y. Wu, X. Peng, B. Guo, J. Fan, Z. Zhang, J. Wang, A. Cui and Y. Gao, *Org. Biomol. Chem.*, 2005, **3**, 1387.
- (a) J. Wu, W. Liu, J. Ge, H. Zhang and P. Wang, *Chem. Soc. Rev.*, 2011, **40**, 3483; (b) T. Mutai, H. Sawatani, T. Shida, H. Shono and K. Araki, *J. Org. Chem.*, 2013, **78**, 2482.
- W. Chen, B. D. Wright and Y. Pang, *Chem. Commun.*, 2012, **48**, 3824.
- R. Y. Tsien, in *In Fluorescent and Photochemical Probes of Dynamic Biochemical Signals inside Living Cells*, ed. A. W. Czarnik, American Chemical Society, Washington, DC, 1993, pp. 130–146.
- (a) M. E. McMennamin, J. Himmelfarb and T. D. Nolin, *J. Chromatogr. B: Anal. Technol. Biomed. Life Sci.*, 2009, **877**, 3274–3281; (b) C. Hwang, A. J. Sinskey and H. F. Lodish, *Science*, 1992, **257**, 1496–1502.
- D. E. Gomez, L. Fabbri, M. Licchelli and E. Monzani, *Org. Biomol. Chem.*, 2005, **3**, 1495–1500.

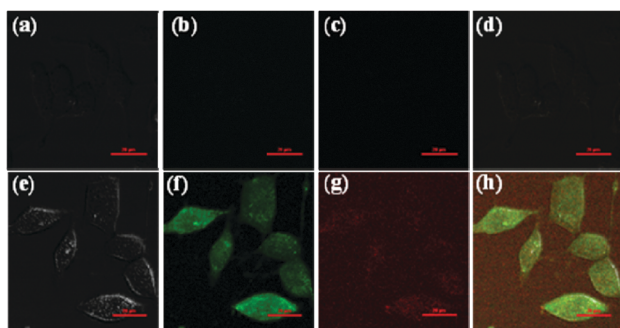


Fig. 4 Fluorescence images of SKOV-3 cells. (a–d) SKOV-3 cells incubated with probe **E1** (10 μM) for 30 min; (e–h) images of cells after treatment with probe **E1** (10 μM) for 30 min and subsequent treatment of the cells with 50 μM Zn^{2+} for 20 min. (a and e) Bright-field images of the SKOV-3 cells in samples; (b and f) images taken in green field; (c and g) images taken in red field; and (d and h) the overlap of brightfield and fluorescence. Scale bar: 20 μm .